Pergamon

Journal of Structural Geology, Vol. 17, No. 2, pp. 293 to 300, 1995

0191-8141/95 $9.50 + 0.00

0191-8141(94)00050-6

Mode of internal deformation in sand wedges

HEMIN KOYI

The Hans Ramberg Tectonic Laboratory, Institute of Earth Sciences, Uppsala University, Norbyvägen 18B, S-752 36 Uppsala, Sweden

(*Received* 19 *January* 1993; *accepted in revised form* 25 *March* 1994)

Abstract—Sequential sections of a sand box model are used to quantify displacement along imbricate surfaces and their rotation and volume loss history within an accreting sand wedge. Model results show that both displacement along the imbricate surfaces and compaction of the imbricate sheets decrease with sequential accretion of the wedge. The model wedge propagates episodically along a basal décollement when displacement along the imbricate surfaces decreases dramatically due to their back rotation and steepening. During their back rotation, the model imbricate sheets undergo compaction which resulted in an area loss of 12–13%, while the entire model shows 17% area loss.

Back rotation of model imbricate sheets takes place in a domino-type style that is accommodated by ductile deformation of sand layers at deeper levels. Deeply located sand layers undergo 40–50% layer parallel shortening compared to no layer parallel shortening of the shallow located layers within the same imbricate sheet. Model sand wedge does not grow self similarly but rather its length/height ratio increases episodically with deformation.

INTRODUCTION

In recent years sand box models have been increasingly used to study different geometric and dynamic aspects of accretionary prisms (Davis *et al.* 1983, Dahlen *et al.* 1984, Karig 1986, Zhao *et al.* 1986, Mulugeta & Koyi 1987, 1992, Mulugeta 1988, Colletta *et al.* 1991, Liu *et al.* 1992, Koyi *et al.* 1992). Davis *et al.* (1983), Dahlen *et al.* (1984) and Dahlen (1984, 1990) presented a comprehensive study on the dynamics of accretionary wedges and compared them to deformation of sand or snow in front of a bulldozer. In an earlier paper, Mulugeta & Koyi (1992) described the episodic accretion history of a sand wedge. In this paper, I focus on the volume loss history and on the significance of internal deformation of the wedge on its propagation. The sand box model described here is deformed on a smooth and rigid décollement and therefore does not account for the natural décollement slope or irregularities. Effects of sedimentation and erosion are not considered in this study.

MODEL DESCRIPTION AND DEFORMATION

A single model consisting of passively layered sand was shortened from one end above a rigid décollement of Plexiglas (for more details of the model see Mulugeta & Koyi 1992). The model contained colored thin layers of sand with a total thickness of 5 mm (Fig. 1a). Profiles were eroded for photographing at intervals during model deformation by using a vacuum cleaner to expose cross-sections. This sequential sectioning enabled detailed monitoring of the model throughout the deformation. Thus, bed lengths, layer thicknesses, amount of displacement along the imbricate surfaces and their dip and wedge slope are all calculated from these sequentially eroded profiles.

During the shortening of the model, a wedge formed that comprised many imbricate sheets. The early imbricate sheets that were closely spaced formed as conjugate kink folds whose forelimb narrowed with further shortening to thrust eventually (Mulugeta & Koyi 1992). As the model was shortened, the wedge grew both in height and length as new imbricate sheets were accreted at its toe. After 3% shortening, the wedge was already twice as thick as the initial thickness of the model.

Model imbricate surfaces defined discrete zones at shallow levels which passed downwards into a wider zone of ductile deformation at depth (Fig. 1b). These imbricate surfaces became sigmoidal in geometry with progressive shortening.

During model shortening, individual sand layers deformed by folding and thrusting and underwent layer parallel shortening. The model wedge and its individual imbricate sheets underwent area loss during model deformation. In order to quantify internal deformation of the model wedge, layer parallel shortening within the sand layers and area loss within the wedge were calculated using bed length and area balancing.

SECTION BALANCING

Strain partitioning

Bed length balancing throughout model deformation was carried out for two single layers at different stratigraphic levels (Figs. 1 and 2). This was done by comparing the length of a layer within an imbricate sheet at the onset of the formation of the imbricate with its length at later stages of the deformation of the imbricate. The measurements show that layer-parallel shortening dominated the deformation at the early stages of model deformation for both the deep and the shallow layers (Fig. 2). At later stages, layer parallel shortening main-

tained its dominance relative to both folding and imbrication for the layer located at deeper levels (Fig. 2a), while imbrication dominated the deformation style with progressive shortening for the shallow layer (Fig. 2b). This contradicts Liu & Dixon's (1991, 1992) findings that folding dominated at high levels and faulting at depth in models using non-Newtonian materials. In the current model, even at shallow levels, total layer-parallel shortening increased periodically just before the formation of a new imbricate in front of the propagating wedge (Fig. 2). This implies that the layers in the front of a propagating wedge deform by layer-parallel shortening before the eventual formation of a conjugate fold box whose forelimb sheared and localized to an imbricate.

This variation in magnitude of deformation components was also apparent within individual imbricate sheets. At shallow levels, layers within individual imbricate sheets underwent no or little penetrative deformation compared to their deeply located equivalents (Fig. 3). At 47% bulk shortening, a layer located at deeper levels within an imbricate was shortened to 55% of its length during deformation of the model (Fig. 3). This decrease in bed length is mainly accommodated by thickening of the layer and partly by area loss due to compaction (see later). This deformation at deeper levels accomplishes domino-type rotation of imbricate sheets. Contrarily, a layer located at shallow levels underwent no layer-parallel thickening during the same period of deformation (Fig. 3). The model therefore resembles variations in deformation style with depth that are likely to occur in nature.

Area loss history

In order to quantify the compaction and area loss within the wedge, the area of three imbricates (numbers 5, 6 and 7 in Fig. 1c) was measured throughout the deformation (Fig. 4). Individual imbricate sheets underwent area loss (and perhaps volume loss) due to their compaction during progressive shortening of the model. Compaction of the imbricate sheets dominated at the beginning of their formation and decreased significantly at later stages (Fig. 4). In fact, as they matured, the imbricate sheets showed very little change in area. Area loss for individual imbricates was calculated as follows:

$$\text{Area loss } \% = (\Delta A_5 + \Delta A_6 + \Delta A_7)/(A_{i5} + A_{i6} + A_{i7})$$

where A_5, A_6 and A_7 are areas of imbricate numbers 5, 6 and 7, respectively (Fig. 1), and A_i is the area of the imbricate sheets immediately after their formation. The total area loss calculated from the measurements was 13%. It is important to mention that there can be a slight increase in volume due to localized back thrusting at the rear of the wedge. However, these back thrusts did not effect those three imbricates that were used in the measurements. Nevertheless, this volume change is negligible compared to the total bulk compaction.

The area loss within the whole wedge was measured in three ways. First, the wedge area was measured during the period between the formation of two imbricate sheets; the wedge area was measured starting from the time of formation of imbricate number 4 (at the onset of the formation of imbricate 4) until the formation of imbricate number 5. The measurements show that during that period, the wedge compacted and lost area by 12.5% (Fig. 4). Second, similar measurements were conducted for the wedge area at the onset of formation of imbricate number 6 throughout the deformation until the formation of imbricate number 7. These measurements showed that the wedge lost an area of 11.7% during that period. Third, the cross-sectional area of the model was measured at the final stage of model deformation and compared to the undeformed cross-sectional area and showed 17% area loss at 47% shortening.

These measurements show that area loss of 12–17% within the wedge and the individual imbricate sheets is approximately constant throughout model deformation. This constant area loss could be attributed to the absence of lateral variation in the sand property. However, in the presence of lateral inhomogeneities which is likely to occur in nature, the area loss may vary during the deformation.

DISPLACEMENT

Ellis & Dunlap (1988) studied the change in displacement along individual thrust faults and concluded that slip varies along the thrust surface with the maxima at the point of nucleation. Ellis & Dunlap's (1988) approach is different from that outlined here where we measure the displacement of a certain horizon along several imbricate surfaces. In this study, displacement of a single, shallow-located layer (A in Fig. 1b) along four imbricate surfaces (numbers 4, 5, 6 and 7 in Fig. 1b) was measured throughout model deformation (Fig. 5). These measurements show that displacement along the imbricate surfaces increased with bulk shortening at the beginning of model deformation and decreased dramatically later during formation of new imbricates (Fig. 5). Our findings are in agreement with the conception that imbricate thrusts develop serially with early thrusts becoming inactive as new ones develop in front of them. However, in their models with microlaminate layers, Liu & Dixon (1991, 1992) showed that displacement along the older imbricates increased with time. They concluded that slip along older thrusts does not die out or cease as new imbricates form in front of them. This difference could be mainly due to the difference in materials which were used in the experiments.

New imbricate surfaces are new deformational sites where most of the displacement is taken up. The measurements show that movement along imbricate number 4 ceased totally during and exactly before the initiation of a new imbricate sheet (imbricate number 5) in front of it at 15–20% bulk shortening (Fig. 5). This stage of little or no increase in displacement with increasing total shortening was followed by renewed movement (at 20–23% bulk shortening) as imbricate number 4 back rotated due to step up of imbricate

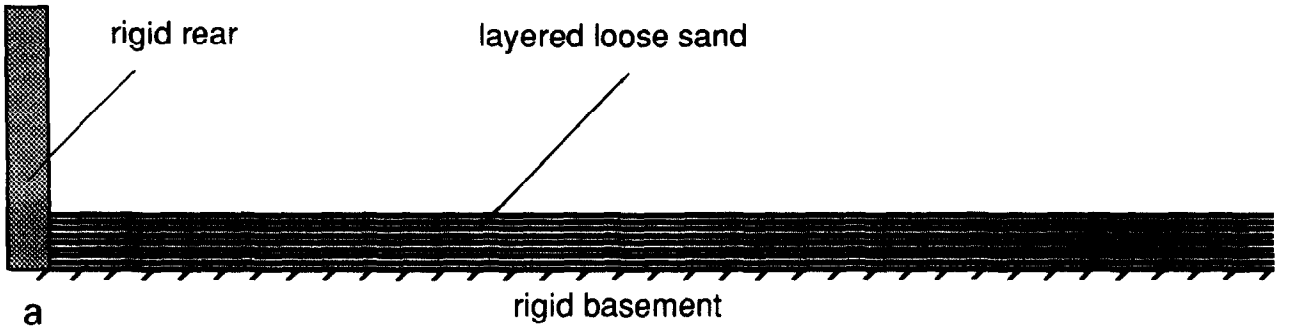

a

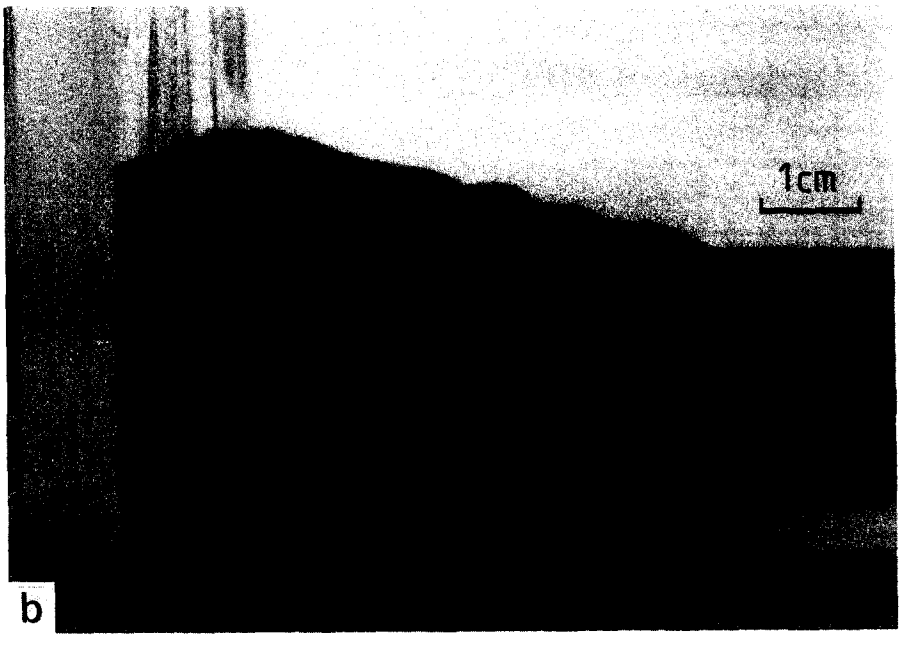

b

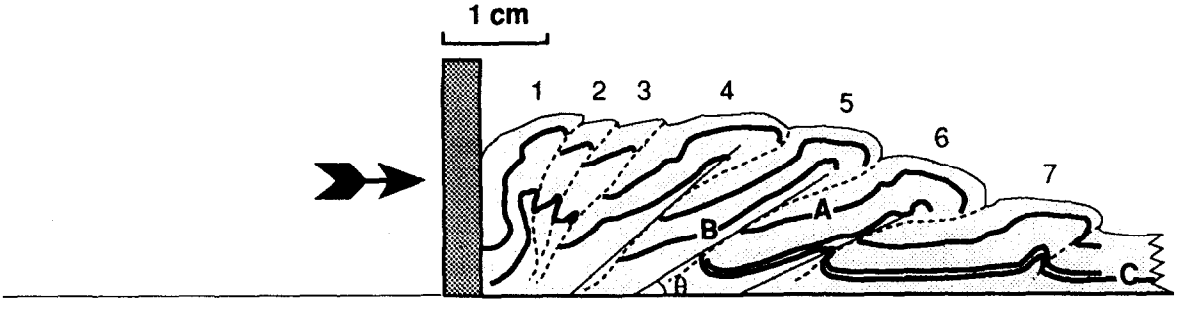

c

Fig. 1. (a) Schematic diagram of initial model set up (not to scale). (b) Model profile at 44% shortening showing the geometry of the imbricate surfaces. Scale bar is 1 cm. (c) A line drawing of model profile in b. (A), (B) and (C) are three passive sand layers which were used for measurements. Dashed lines are imbricate surfaces which possess a sigmoidal geometry. The dip of their planar parts are shown by the straight lines. The numbers denote the sequence at which the imbricates formed.

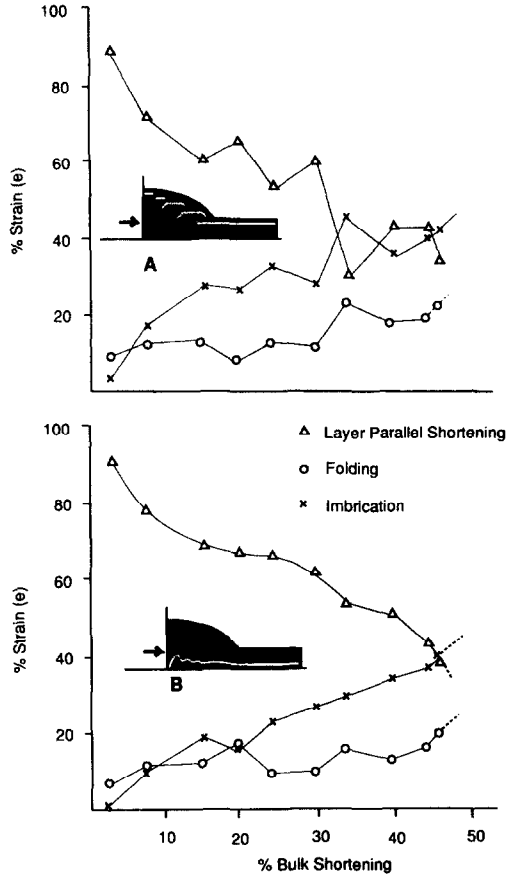

Fig. 2. Strain partitioning of two layers located at two stratigraphic levels in the model. Note that in the shallow layer (A), imbrication dominates deformational style after 30% bulk shortening. Also note that change in layer-parallel shortening in the shallow layer is periodic corresponding to stages before the formation of new imbricates. In the deeper layer (B), layer parallel shortening dominates until 45% bulk shortening and maintains a smoother curve.

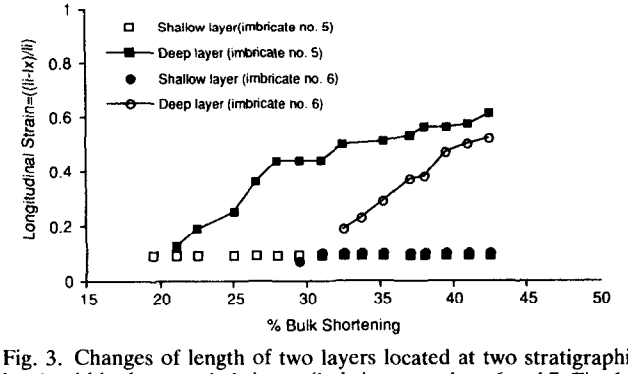

Fig. 3. Changes of length of two layers located at two stratigraphic levels within the same imbricates (imbricate numbers 6 and 7, Fig. 1c) throughout the deformation. Note that the shallow layer in both imbricates undergoes no length change throughout the deformation of the imbricates. The deep layers, on the other hand undergo continuous shortening and layer-parallel shortening with the deformation of the individual imbricates.

number 5 in front of it. At this stage, imbricate number 4 had reached the position where it could not back rotate any further and movement along it was almost totally ceased (Fig. 5). The same is true for imbricate number 5 where total displacement along it increased continuously until the initiation of imbricate number 6. At this

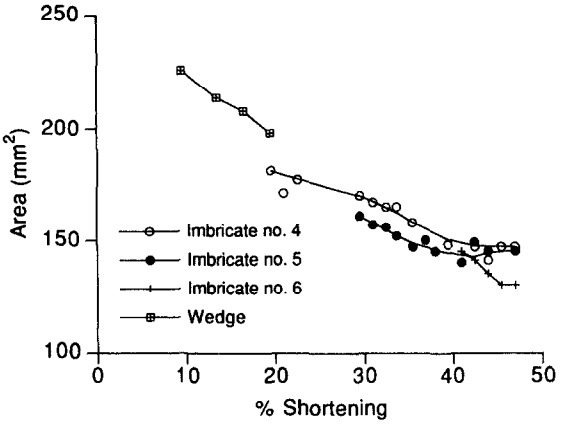

Fig. 4. Measured area loss within the wedge and the last three individual imbricates (numbers 5, 6 and 7) vs shortening.

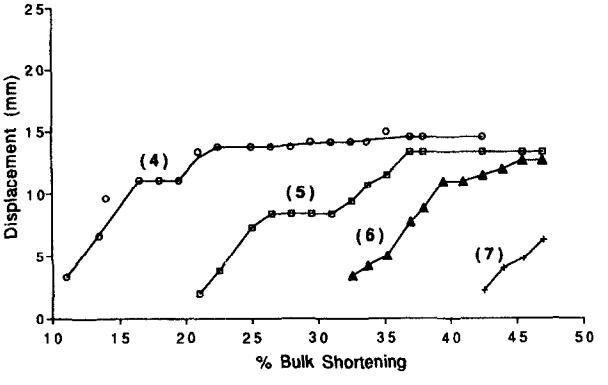

Fig. 5. Measured displacement along the four last imbricates (4, 5, 6 and 7) in the model. Note that displacement along all of the imbricates follow a similar pattern; starting with sharp increase as the imbricate begins to form, followed by little or no additional displacement before the formation of a new imbricate in front of them. This in turn is followed by a gentler increase in the displacement that decreases dramatically later with progressive deformation.

stage, movement along the imbricate surface (number 5) ceased and most of the push from the rear was taken up along the new imbricate surface (number 6). Step up thickening of new imbricates result in back rotation of the older imbricate surfaces. The degree of rotation and relative displacement along the imbricate surfaces decreases with age and distance from the newly formed imbricate.

Figure 5 also shows that total displacements along imbricate surfaces reach a constant amount after a certain bulk shortening. This supports earlier conclusions by Mulugeta & Koyi (1987) that the imbricates are added to a flat topped domain at the back of the wedge where no significant movement along the imbricate surfaces is taking place any more. The striking observation of Fig. 5 is that the total displacement along the imbricate surfaces ranges between 13–15 mm. This may imply that once the spacing of the imbricate is close and no inhomogeneities are produced, the total displacement along the imbricate surfaces remain similar.

Steepening and back rotation of imbricate sheets

Rotation of imbricate surfaces (thrusts) in sand box experiments is reported by Mulugeta & Koyi (1987, 1992), and Liu *et al.* (1992). Liu *et al.* (1992) reported that older thrusts are back-rotated to 45° where they were involved in the vertical uplift zone at the back of the wedge. In our models, the older imbricate surfaces back-rotated to nearly upright positions (Fig. 1b and fig. 7 in Mulugeta & Koyi 1992). In fact, in Liu *et al.*'s (1992) models (their fig. 6), the oldest imbricate surfaces back-rotate to almost upright position. Liu *et al.*'s (1992) models show that in the initially thinner models where, more imbricate sheets formed, the imbricate surfaces back rotated to steeper positions than their equivalents in the thicker models.

When new imbricates form in front of them, the older imbricates rotate backward and steepen with progressive deformation. As most of the deformation is occurring along the youngest imbricate, rotation and steepening of this imbricate surface results in a decrease of the displacement along it (Fig. 5). Consequently, any further push from the rear causes internal deformation of the wedge and/or slip along the basal décollement.

Backward rotation of the model imbricate sheet is accommodated by relative slip along imbricate surfaces as in a stack of blocks rotating around separate points on the same line. Back rotation of the imbricates is similar to domino-type rotation. But in this case, the imbricates do not rotate as totally rigid blocks. Their back rotation cause slip along discrete imbricate surface at shallow levels and ductile strain at the deeper levels (Figs. 2 and 3). Back rotation of the younger imbricates causes compaction and thickening of the wedge which accommodate only very small amount of the total deformation.

Steepening of natural imbricate surfaces is reported from Moine thrust zone in northwest Scotland and Arr massive in the Alps (Boyer & Elliott 1982). Boyer & Elliott (1982) reported that the dip of thrusts in the Moine thrust zone ranges between 25–55° with the shallow dipping thrusts to the northeast of the zone (i.e. forelandwards) across strike. Using geophysical data and surface geology, Butler & Coward (1984) drew thrust geometries within the Moine thrust belt. In their cross-sections (figs. 5 and 11) they showed steepening of imbricate thrusts hinterwards both within the Moine nappe and in the zone below the Moine thrust. Butler (1987) hypothetically illustrated the steepening and back rotation of older thrusts by subsequent development of new thrusts in their footwall and suggested that they experience a longer straining history.

DISSIMILARITY

Although, boundary conditions were kept constant and no material was added or eroded from the model, the wedge did not grow self similarly as it is suggested for natural accretionary wedges (Fig. 6). Instead, wedge growth was episodic and its length/height ratio varied

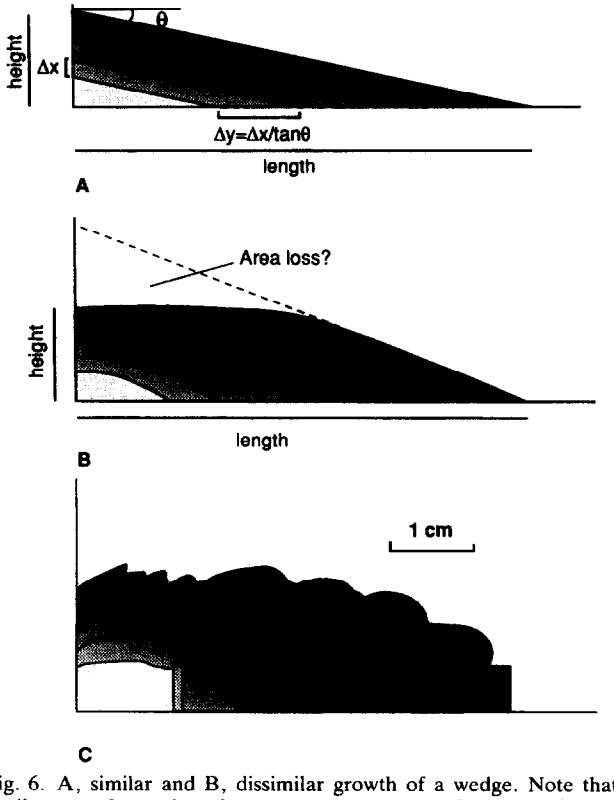

Fig. 6. A, similar and B, dissimilar growth of a wedge. Note that similar growth requires that a constant amount of material (Δx) is added to the height of the wedge when the length of the wedge increases by a constant amount (Δy). C, is an outline of the model wedge at several stages of its deformation showing its dissimilar growth. The increase in height of the model wedge is significantly smaller than its length.

with shortening (Figs. 6 and 7). This dissimilar growth may be due to change in rheology of the sand which was compacted during deformation of the model. At the early stages of the deformation, vertical wedge growth is rapid relative to its lateral growth (Figs. 7b & c). With progressive shortening however, the wedge grew in length significantly faster than its height. In fact, vertical growth of the wedge was significantly small at the later stages of deformation (Fig. 7a). Any addition to the length of the wedge due to material accretion at the toe caused smaller growth of its height (Fig. 7). Simple measurements of Colletta *et al.*'s (1991) model (their fig. 5) shows that for the same amount of shortening wedge length/wedge height ratio increases from 3 to 4.17 when the basal friction is decreased. Figures 7(a) & (b) show that with the formation of a new imbricate the length/height ratio increases rapidly. Thereafter, (i.e. after each stage of step up of a new imbricate sheet) the length/height ratio declines gently suggesting that the actual length of the wedge decreases between two periods of step up (Figs. 7a & b). This decline is mainly due to lateral compaction within the new imbricate and/or increase of the wedge height (Fig. 7, and see Mulugeta & Koyi 1992). Similar curve for Colletta *et al.*'s (1991) and Liu *et al.*'s (1992) available cross-sections of their sand models also shows that the length/height ratio increases with deformation (Figs. 7c & d).

If the wedge is divided to two main domains, a flat topped domain (area A in Fig. 8) and a domain of sole

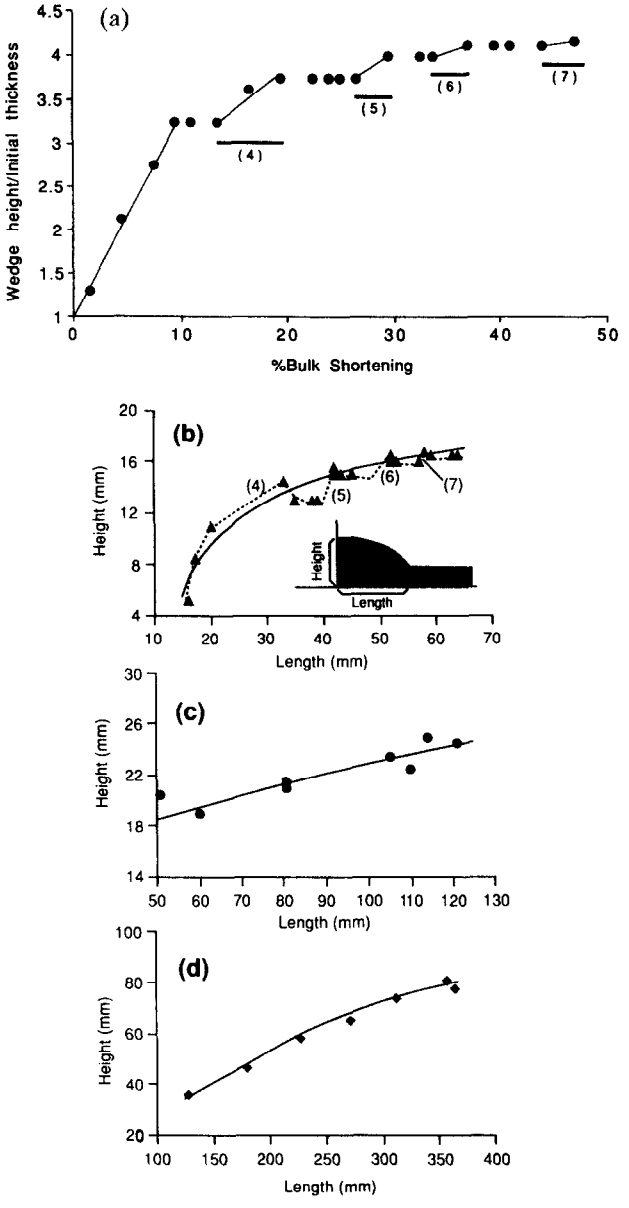

Fig. 7. (a) Vertical growth of model wedge with shortening. Bars indicate stages just before the formation of a new imbricate in front of the wedge. The sharp slope of the curve indicates rapid vertical growth of the wedge at the early stages of the deformation to reach a critical taper. Length/height ratio of (b) the current model wedge with progressive shortening, (c) Colletta *et al.*'s (1991) model, (d) Liu *et al.*'s (1992) model. The numbers in (a) correspond to imbricate step up stages where the length of the wedge increases rapidly due to formation of new imbricate sheets. Note that the total increase in wedge length is higher than the total increase of its height.

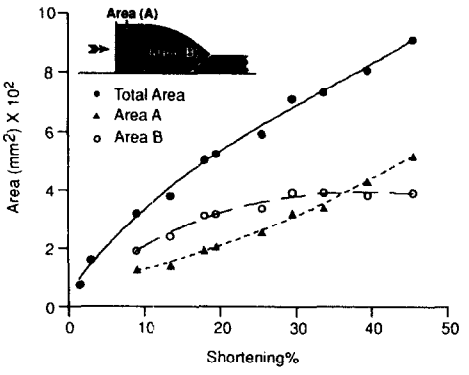

Fig. 8. Total wedge growth with shortening. Note that the flat-topped domain (area A) grows with shortening while area (B) stops growing after certain percentage shortening when a critical taper is reached.

thrust propagation and back rotation (area B in Fig. 8), domain B grows continuously with time until a taper is formed (Fig. 8). If boundary conditions, material properties and model kinematics were kept constant, domain B maintains a constant area (volume?) with further shortening. On the other hand, domain A grows with time as rotated and compacted imbricates are added to it (Fig. 8).

DISCUSSION

At the early stages of model deformation, the wedge underwent internal deformation and grew rapidly in order to reach a critical taper. Evidence for this is that at 9% shortening, the wedge had a lateral extent (parallel to the shortening direction) of only 8.6% of the initial length of the model and it was 2.5 times as thick as the initial thickness of the model compared to 9% of initial length and twice as thick as the initial thickness at 3% bulk shortening. This internal deformation is a complementary process to build up a critical wedge taper which could transmit further push from the rear and overcome the basal friction.

In the model, at a certain increment of time, push from the rear was mostly taken up by movement along the youngest of the imbricate surfaces. Older imbricates accommodate only small part of the displacement (Fig. 5). Boyer & Elliott (1982) suggested that as the slip transferred to a new lower thrust, a portion of the major thrust is de-activated and rides passively within the growing thrust sheet. We think that the older imbricates remain relatively active until they rotate to their locking position.

The model wedge grows both in height and length with progressive shortening. This growth is very rapid at the early stages of the deformation as a critical taper is forming (Fig. 7a). At later stages of the deformation however, the growth in length of the wedge persists but at a slower rate. Relatively rapid vertical growth of the wedge however, decreases dramatically after the critical taper is reached (Fig. 7a). At later stages of model deformation when younger imbricates are accreted at the toe, the height of the wedge increases stepwise in small amounts giving it a gentle increase with deformation (Figs. 7a & b). Expectedly, each of these steps predates the formation of a new imbricate (Figs. 7a & b). This implies that for the wedge to overcome the basal friction, it undergoes thickening until it again reaches a critical taper that can overcome the basal friction and brings about slip along the décollement. Another interesting observation is that when a critical taper is attained, only a small amount of vertical growth of the wedge is needed to continue gliding along the décollement (Fig. 7a). These results are strongly dependent on the boundary conditions and rheology of the materials added to the wedge. Any change in the basal friction and

inhomogeneity in the materials added to the wedge may dramatically change the geometry of the critical taper.

At later stages of model deformation, compaction (area loss) within the imbricate sheets and displacement along their surfaces decreased dramatically (Figs. 4 and 5) supporting the suggestion that a relatively inactive flat-topped domain builds up at the back of the model where little deformation takes place (Mulugeta & Koyi, 1987). Further push is accommodated by displacement along the younger imbricate surfaces and compaction within domain B (Fig. 8). After being rotated and compacted, the imbricates are added to the flat-topped domain that increases in area with progressive shortening (Fig. 8). This flat-topped domain could deform by a few back thrusts that formed at the back of the model. However, in the current model, the few back thrusts that formed at a later stage of model deformation were localized within a small part of the back of the model. The relatively small increase in the height of the wedge (Fig. 8) could be attributed to the movement along these back thrusts.

In general, the individual imbricate sheets underwent an area loss of 12–13% during the shortening of the model. But, bed length balancing of sand layers at two different levels within the same imbricate sheet shows that the deeper sand layer shortened by 55% of its initial length (Fig. 3) whereas the shallow layer kept its initial length after the same shortening period. The shortening of the deeper layer is mainly taken up by thickening of the layer and partly by area loss. This suggests that the area loss within the model imbricate sheets is dominant at deeper levels and decreases significantly at shallower levels where the sand layers do not show any penetrative strain.

Change in rheology of the model sand due to its compaction during model deformation, could account for the dissimilar growth of the model wedge and its high taper (16–20°) than the estimated theoretical value (6–10°).

CONCLUSIONS

Results of a sand model shortened above a rigid décollement, show that:

(1) Ductile deformation dominates at deep levels and allows domino-type back rotation of the older imbricates with progressive deformation.
(2) Displacement along imbricate surfaces are equal if they possess similar spacing.
(3) During their back rotation and compaction, model imbricate sheets undergo area loss which could be one of the reasons for the dissimilar growth of the wedge. Area loss within model imbricate sheets is dominated at deeper levels.
(4) During progressive deformation, model accretionary wedges exhibit dissimilar growth rather than growing self similarly.

Acknowledgements—Sincere thanks are due to Genene Mulugeta for insightful discussions and for commenting on the manuscript. Ruud Weijermars, Steve Laubach and Steve Seni are thanked for reading and commenting on earlier versions of the manuscript. Comments of two anonymous referees are greatly appreciated. This paper was improved by comments and suggestions of Dr Steven F. Wojtal. Funded by the Swedish Natural Research Council (NFR).

REFERENCES

Boyer, S. E. & Elliott, D. 1982. Thrust systems. *Bull. Am. Ass. Petrol. Geol.* **66**, 1196–1230.
Butler, R. W. H. 1987. Thrust sequences. *J. geol. Soc.* **144**, 619–634.
Butler, R. W. H. & Coward, M. P. 1984. Geological constraints, structural evolution, and deep geology of the northwest Scottish Caledonides. *Tectonics* **3**, 347–365.
Colletta, B., Letouzey, J., Pinedo, R., Ballard, J.F. & Balé, P. 1991. Computerized X-ray tomography analysis of sandbox models: examples of thin-skinned thrust systems. *Geology* **19**, 1063–1067.
Dahlen, F. A., Suppe, J. & Davis, D. M. 1984. Mechanics of fold-and-thrust belts and accretionary wedges (continued): Cohesive Coulomb Theory. *J. geophs. Res.* **89**, 10,087–10,101.
Dahlen, F. A. 1984. Noncohesive critical Coulomb wedges: and exact solution. *J. geophs. Res.* **89**, 10,125–10,133.
Dahlen, F. A. 1990. Critical taper model of fold-and-thrust belts and accretionary wedges. *Ann. Rev. Earth & Planet. Sci.* **18**, 55–99.
Davis, D., Suppe, J. & Dahlen, F. A. 1983. Mechanics of fold-and-thrust belts and accretionary wedges. *J. geophys. Res.* **88**, 1153–1172.
Ellis, M. A. & Dunlap, W. J. 1980. Displacement variation along thrust faults: implications for the development of large thrusts. *J. Struct. Geol.* **10**, 183–192.
Karig, D. E. 1974. Evolution of arc systems in the Western Pacific. *Ann. Rev. Earth & Planet. Sci.* **2**, 51–75.
Karig, D. E. 1986. Physical properties and mechanical state of accreted sediments in the Nankai Trough, Southwest Japan. Arc. *Mem. geol. Soc. Am.* **166**, 117–133.
Koyi, H., Vendeville, B. & Mulugeta, G. 1992. Dissimilar growth of accretionary wedges; examples from sand experiments. *Geol. Soc. Am. Prog. w Abs.* **A245**.
Liu, S. & Dixon, J. M. 1991. Centrifuge modelling of thrust faulting: strain partitioning and sequence of thrusting in duplex structures. In: *Deformation Mechanisms, Rheology and Tectonics* (edited by Knipe, R. J. & Rutter, E. H.). *Spec. Publ. geol. Soc. Lond.* **54**, 431–444.
Liu, S. & Dixon, J. M. 1992. Centrifuge modelling of the propagation of thrust faults. In: *Thrust Tectonics* (edited by McClay, K.). 53–69.
Liu, H., McClay, K. R. & Powell, D. 1992. Physical models of thrust wedges. In: *Thrust Tectonics* (edited by McClay, K.). 71–81.
Mulugeta, G. 1988. Modelling the geometry of Coulomb thrust wedges. *J. Struct. Geol.* **10**, 847–859.
Mulugeta, G. & Koyi, H. 1987. Three-dimensional geometry and kinematics of experimental piggyback thrusting. *Geology* **15**, 1052–1056.
Mulugeta, G. & Koyi, H. 1992. Episodic accretion and strain partitioning on a model sand wedge. *Tectonophysics* **202**, 319–333.
Zhao, W. L., Davis, D. M., Dahlen, F. A. & Suppe, J. 1986. Origin of convex accretionary wedges: evidence from Barbados. *J. geophys. Res.* **91**, 10,241–10,258.